blood®
Regular Article

HEMATOPOIESIS AND STEM CELLS

An in vivo barcoded CRISPR-Cas9 screen identifies *Ncoa4*-mediated ferritinophagy as a dependence in *Tet2*-deficient hematopoiesis

Justin Loke,[1,2,*] Peter G. Kim,[1,3,*] Thuy T. P. Nguyen,[4] Meaghan Boileau,[5] Marie McConkey,[1] Aidan Miller,[1] Wesley Shin,[1] Christopher B. Hergott,[1,6] Maria Ericsson,[7] Anja Nordstrom,[7] Paula Montero Llopis,[8] Scott A. Armstrong,[5] Joseph D. Mancias,[4] and Benjamin L. Ebert[1,9]

[1]Department of Medical Oncology, Dana-Farber Cancer Institute, Boston, MA; [2]Institute of Cancer and Genomic Sciences, University of Birmingham, Birmingham, United Kingdom; [3]Cancer Center, Mass General Research Institute, Massachusetts General Hospital, Boston, MA; [4]Department of Radiation Oncology and [5]Department of Pediatric Oncology, Dana-Farber Cancer Institute, Boston, MA; [6]Department of Pathology, Brigham and Women's Hospital, Boston, MA; and [7]Department of Cell Biology and [8]MicRoN Core, Harvard Medical School, Boston, MA; and [9]Broad Institute, Cambridge, MA

KEY POINTS

- **A barcoded in vivo CRISPR-Cas9 KO screen identifies *Ncoa4* as a dependency in *Tet2*-mutant HSPCs.**
- **In *Tet2*-mutant stem and progenitor cells, NCOA4 maintains iron availability for increased mitochondrial adenosine triphosphate production.**

***TET2* is among the most commonly mutated genes in both clonal hematopoiesis and myeloid malignancies; thus, the ability to identify selective dependencies in *TET2*-deficient cells has broad translational significance. Here, we identify regulators of *Tet2* knockout (KO) hematopoietic stem and progenitor cell (HSPC) expansion using an in vivo CRISPR-Cas9 KO screen, in which nucleotide barcoding enabled large-scale clonal tracing of *Tet2*-deficient HSPCs in a physiologic setting. Our screen identified candidate genes, including *Ncoa4*, that are selectively required for *Tet2* KO clonal outgrowth compared with wild type. Ncoa4 targets ferritin for lysosomal degradation (ferritinophagy), maintaining intracellular iron homeostasis by releasing labile iron in response to cellular demands. In *Tet2*-deficient HSPCs, increased mitochondrial adenosine triphosphate production correlates with increased cellular iron requirements and, in turn, promotes Ncoa4-dependent ferritinophagy. Restricting iron availability reduces *Tet2* KO stem cell numbers, revealing a dependency in *TET2*-mutated myeloid neoplasms.**

Introduction

Loss-of-function mutations in *TET2* are commonly found in clonal hematopoiesis of indeterminate potential (CHIP) and hematologic malignancies, including myelodysplastic syndrome (MDS) and acute myeloid leukemia (AML).[1] CHIP is maintained over the lifetime of an individual,[2] consistent with the presence of driver mutations in hematopoietic stem cells (HSCs).[3] TET2 is an iron- and 2-oxoglutaric acid–dependent enzyme that catalyzes the oxidation of methylcytosine, resulting in demethylation of the cytosine residue.[4] Conditional knockout (KO) modeling of *Tet2* in the murine hematopoietic system faithfully recapitulates clonal expansion observed in CHIP through increased HSC renewal and premalignancy.[5,6]

Both CHIP and normal HSCs reside in a specialized bone marrow (BM) niche with specific nutrient availability, cellular interactions, and cytokine and chemokine exposure.[7-10] HSCs with CHIP mutations may remodel BM microenvironments and depend on secreted factors at precise concentrations for their expansion.[11-13] Genetic screens have the ability to identify selective dependencies in somatically mutated cells, and in vivo screens have the potential to access aspects of normal and neoplastic biology that exist only within the native HSC microenvironment. A central challenge of such screens is the tremendous diversity of differentiation and proliferative potential of hematopoietic stem and progenitor cells (HSPCs).[14-18] This challenge of cellular heterogeneity in an in vivo CRISPR-Cas9 screen can be addressed using barcoding strategies to track simultaneously the clonal progeny of each virally transduced HSPC clone and the corresponding effect of the single-guide RNA (sgRNA)-mediated genetic perturbation.

In this study, we developed an in vivo barcoded CRISPR-Cas9 screening methodology to identify genetic dependencies in HSPCs and applied this technique to identify novel regulators of *TET2*-mutant expansion in a model of CHIP. We provided orthogonal validation using a genetic KO mouse model and pharmacologic manipulation of the target pathway. Finally, we used both in vivo and in vitro experiments in primary mouse and human HSPCs to provide a rationale for the synthetic lethal

vulnerability observed in *TET2* KO compared with wild-type (WT) HSPCs.

Methods

Barcoded CRISPR-Cas9 sgRNA library construction

Barcoded libraries were constructed by cloning unique molecular identifiers (UMIs) into the KflI site of the CROPseq-guide-puro vector using Gibson Assembly (New England Biolabs).[19] Custom libraries targeting all transcription and chromatin factors were generated based on previously established lists.[20,21] sgRNAs were picked using the GUIDES algorithm.[22] Lentiviral particles were generated via transfection of HEK293T cells using FuGENE (Promega). Viral constructs were cotransfected with pMD2.G (plasmid 12259; Addgene) and psPAX2 (plasmid 12260; Addgene), and lentiviral particles were harvested 2 to 3 days after transfection.

BM was isolated from B6J.129(Cg)-Gt(ROSA)26Sortm1.1(CAG-cas9*,-EGFP)Fezh/J (Jax 026179) bred to the Vav-Cre + Tet2 fl/fl or control Vav-Cre + background. After euthanasia, BM was stained with CD117 microbeads (Miltenyi Biotec) and CD117-expressing BM was purified by magnetic column selection. Lineage$^-$Sca1$^+$cKit$^+$ (LSK) HSPC or CD150$^+$CD48$^-$CD34$^-$CD135$^-$LSK (HSC) antibody cocktail (see supplemental Table 8, available on the *Blood* website) was used to stain CD117$^+$-enriched BM. LSK HSPC or HSC were then purified by fluorescence-activated cell sorting using a Sony MA900 cell sorter. Fluorescence-activated cell sorting–purified HSCs or LSK HSPCs and concentrated viruses were resuspended in polyvinyl alcohol–based medium.[23] Virus generated from HEK293T cells was concentrated via ultracentrifugation for 2 hours at 25 000 rpm before LSK transduction. LSKs were transduced for 30 minutes at 2000 rpm by spinfection in the presence of polybrene (2 μg/mL). After viral transduction, cells were cultured overnight in a humidified incubator at 37°C and subsequently were retro-orbitally injected into lethally irradiated mice (450 cGy × 2) (10 recipients each per genotype per library).

The transduction of HSPCs or HSCs using our UMI-labeled guide RNAs (gRNAs) enables identification of descendants of each initial lentiviral transduced cell in vivo, as identified by an independent UMI shared by their progeny. This technology identifies the number of related clones (clone frequency) that survive to the terminal time point and the change in the size (number of cells) of these clones. These measurements can then be related to the genetic perturbation mediated by the corresponding sgRNA. We subsequently pooled the results from all the mice in the in vivo screen, within the shared experimental conditions, to maintain adequate coverage of the sgRNA library (97% of the genes were represented across the mouse pool at the terminal analysis). Further details and discussion of this analysis are provided in the supplemental Methods and supplemental Figure 1.

Competitive BM transplantation

Whole BM cells from Cd45.1/Cd45.2 were mixed with Tet2 fl/fl;Cd45.2 (Tet2 KO), Ncoa4 fl/fl Cd45.2 (Ncoa4 KO), or Tet2 fl/fl Ncoa4 fl/fl Cd45.2 (Tet2 KO Ncoa4 KO) in phosphate-buffered saline at an 80:20 ratio. In these mice, Cre recombinase expression was driven by either Mx or Vav promoter, depending on the experiments described. Cells were injected retro-orbitally into lethally irradiated B6.SJL-Cd45.1 recipient mice (450 cGy × 2). Induction of Cre recombinase expression in the Mx-Cre models was accomplished by intraperitoneal injection of polyinosinic:polycytidylic acid (high molecular weight) (InvivoGen) 10 mg/kg, for 3 doses on alternate days in Mx-Cre transgenic mice.[24]

The Dana-Farber Cancer Institute Institutional Care and Use Committee reviewed, authorized, and monitors the mouse work used during this study.

Additional methods are enclosed in the supplemental Information.

Results

Identification of synthetic lethal vulnerabilities in *Tet2*-deficient HSPCs

We generated a library of 12 727 sgRNAs targeting 2055 genes (6 sgRNAs per gene) identified as putative epigenetic and transcription factors alongside 354 control sgRNAs. To enable the tracking of the clonal progeny of each cell transduced by a lentivirus, we encoded a nucleotide-based UMI library within the sgRNA-expressing vector, enabling simultaneous clonal tracing of each HSPC transduction event and identification of the corresponding CRISPR-Cas9-mediated genetic perturbation (Figure 1A; supplemental Figure 1A), whereby clonally related descendants from the transduced HSPC would share the same UMI-gRNA. The size of the clone could be inferred from the variant allelic frequency (normalized read depth) of the detected UMI-gRNA.

To investigate the genes that are selectively required for clonal fitness in *Tet2* KO compared with WT cells, we transplanted 4 million Cas9-expressing *Tet2* KO or WT LSK HSPCs, which were transduced with our UMI-labeled sgRNA library, into 40 lethally irradiated recipient mice. The screening platform detected each clone with sufficient sequencing depth, maintained adequate representation of library genes during transplantation, and enabled tracking of >200 000 unique clones with 81 to 137 cells represented per sgRNA (supplemental Figure 1B-F).

We examined BM from mice at 14 weeks after transplant, a time point by which transplanted HSCs contribute to most of the hematopoietic system.[18] We identified 500 to 2500 unique clones per mouse at this terminal analysis (supplemental Figure 1G-H). At this time point, we quantified the number of surviving clones with sgRNA targeting genes compared with control sgRNAs, as a surrogate for HSC potential. Genes known to cooperate with *Tet2* loss to drive hematologic malignancy (eg, *Bcor* and *Tet3*) resulted in an increase in the number of *Tet2* KO clones (Figure 1C). *BCOR* loss-of-function mutations have been identified in *TET2*-mutated MDS,[25] and *Bcor* deletion in Tet2-mutant mouse models results in MDS/myeloproliferative neoplasm.[26] Deletion of *Tet3* has been observed to accelerate the development of *Tet2*-deficient AML in mice.[27]

We next sought to identify genetic dependencies of *Tet2* KO HSPCs. We hypothesized that sgRNA-mediated gene KOs that result in a reduction in both the number (ie, unique clones) and

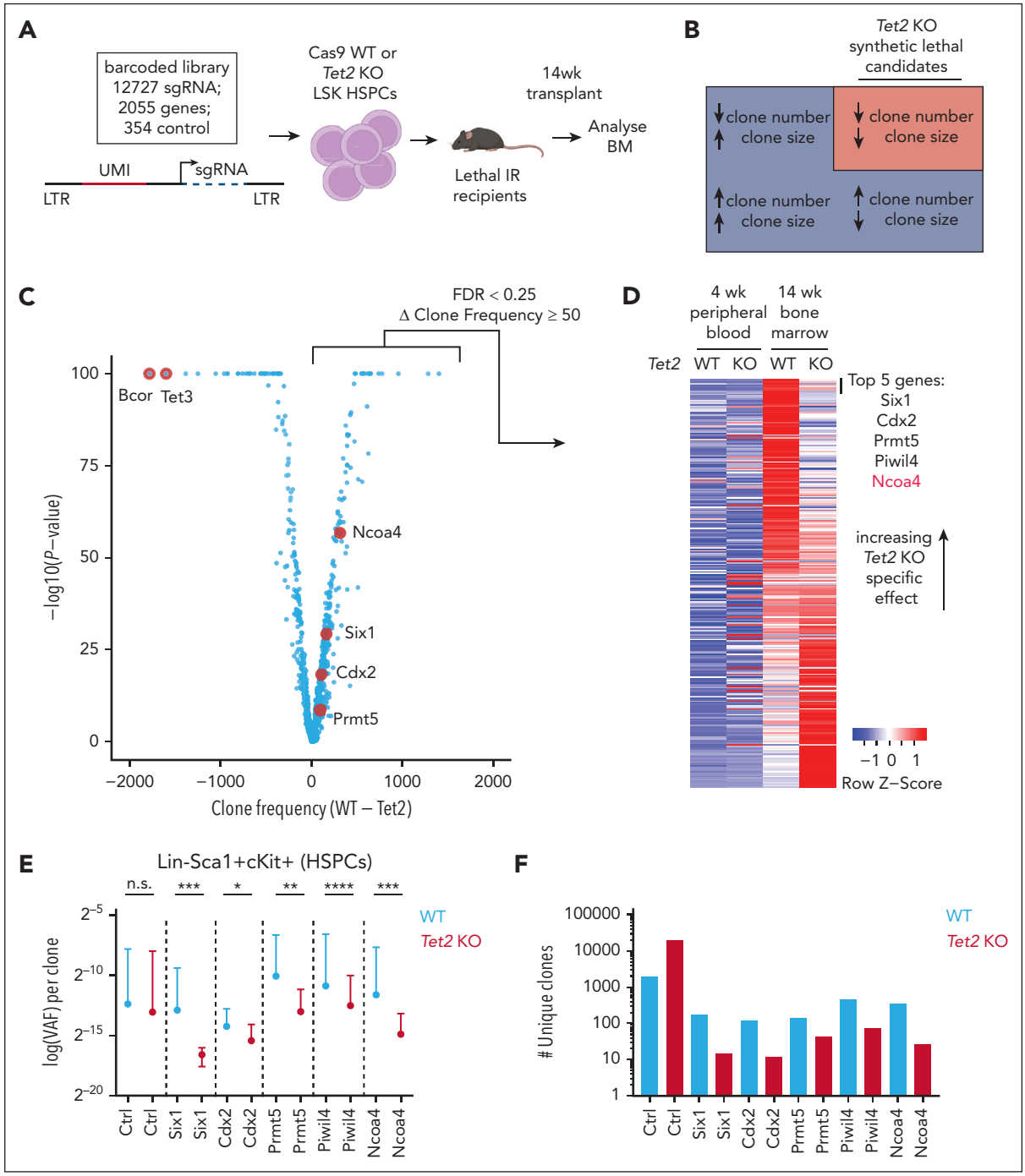

Figure 1. A UMI-barcoded in vivo CRISPR-Cas9 screen identifies synthetic lethal targets of *Tet2* KO–driven expansion of HSPCs. (A) A nucleotide-encoded UMI linked to an sgRNA expression cassette in a lentiviral vector allows clonal tracing after transduction. Lentiviral infection of WT or *Tet2* KO Cas9 expressing murine LSK HSPCs was harvested 14 weeks after transplantation into lethally IR recipients. (B) Analysis strategy to identify genetic dependencies of *Tet2* KO HSPC growth after UMI-based in vivo screening. (C-D) Results of the pooled CRISPR-Cas9 KO screen in *Tet2* KO and WT HSPCs. (C) Candidate genes result in a reduced number of *Tet2* KO clones compared with WT. *P* value was obtained using a Fisher exact test comparing the number of clones containing nontargeting sgRNAs with the number of clones containing gene-specific sgRNAs in WT vs *Tet2* KO. (D) Genes with greater persisting clones in WT (*Tet2* KO–WT clone numbers >50) were subsequently ranked by *Tet2* KO–specific decrease in clone size (variant allelic frequency [VAF]) at 14 weeks, and VAF differences were assessed by Welch's *t* test. Row normalized by z score. All *P* values were adjusted for multiple hypothesis testing via FDR. (E) VAF and (F) clone numbers for the top *Tet2* KO–specific target genes identified in the CRISPR-Cas9 screen. Welch's *t* test: n.s., $^{*}P < .01$; $^{**}P < .001$; $^{***}P < .0001$. FDR, false discovery rate; IR, irradiated; LTR, long-terminal repeat; n.s., nonsignificant.

size (ie, variant allelic frequency, related to the number of cells) (supplemental Figure 1A) of *Tet2* KO clones compared with WT were most likely to represent synthetic lethal vulnerabilities in *Tet2* KO HSPCs (Figure 1B; supplemental Figure 1I; supplemental Table 2). We identified candidate genes that were associated with a reduction in the number of *Tet2* KO clones. Next, we ranked these candidate genes by their effect on *Tet2* KO clone size. Top candidate genes identified by this strategy have recently been shown to contribute to myeloid neoplasia: *Six1*,[28] *Cdx2*,[29] *Piwil4*,[30] and *Prmt5*[31] (Figure 1D-E;

supplemental Figure 1I), showing remarkable predictive power to identify genes required for oncogenesis. Our approach identified genetic dependencies in hematologic cell lines annotated by the Cancer Dependency Map[32] (supplemental Figure 1J). In contrast, we found that analysis by existing pipelines (MAGeCK[33]) misclassifies known tumor suppressor genes as potential *Tet2* synthetic lethal candidates (supplemental Table 3).[34]

Thus, we establish the use of a UMI-barcoded CRISPR-Cas9 in vivo screen to enable clonal tracing over a long-term transplant and thereby robustly identify genetic dependencies in *Tet2* KO HSPCs.

Ncoa4 KO impairs the competitive transplantation advantage of *Tet2* KO HSPCs

To validate the synthetic lethal candidates identified by this screen, we used CRISPR-Cas9 to target 24 top candidate genes in $CD150^+CD48^-CD135^-$LSK HSCs with an independent validation library of sgRNAs. This confirmed that KO of top candidate genes *Cdx2*, *Piwil4*, and *Ncoa4* resulted in a significant detriment to *Tet2* KO HSC clonal competitiveness (supplemental Figure 2A). Having identified and validated putative synthetic lethal targets of *Tet2*-mutant HSPCs, we sought to further investigate *Ncoa4*, a top candidate gene, whose role in both normal and *Tet2*-deficient HSPCs was previously unclear. In particular, we aimed to validate *Ncoa4* as a synthetic lethal target of *Tet2*-mutant HSPCs and understand the underlying impact of *Ncoa4* KO on *Tet2* KO HSPC function. We transduced Cas9-expressing *Tet2* KO or WT HSCs ($CD150^+CD48^-CD135^-$LSK[35]) with lentiviral vectors encoding a fluorescent protein in series with *Ncoa4* or control sgRNA (Figure 2A). This enabled flow cytometry-based tracking of CRISPR-Cas9 modified hematopoietic progeny. This transplantation revealed a progressive reduction in peripheral blood chimerism from *Ncoa4* sgRNA compared with control sgRNA (Figure 2B), which was more pronounced in *Tet2* KO than WT.

We next sought to validate the CRISPR-Cas9 screen results using a transgenic *Ncoa4* KO mouse model.[38] We first used a Cre recombinase regulated by the Vav promoter, which enabled excision of *Ncoa4* and/or *Tet2* starting from the earliest fetal hematopoietic compartments[39] (Figure 2C). By 12 weeks, the expansion of *Tet2* KO blood cells relative to WT cells was reduced in the setting of *Tet2; Ncoa4* double KO (Figure 2D; supplemental Figure 2B). However, there was a reduction in differences in peripheral blood and BM expansion capacity between *Ncoa4* KO; *Tet2* KO and *Tet2* KO in the Vav-Cre driven system at 16 weeks, possibly owing to compensatory CD71 upregulation (Figure 2D; supplemental Figure 2C-D). Despite this compensation, in a secondary transplantation of whole BM, *Tet2; Ncoa4* double KO had reduced repopulating capacity compared with *Tet2* KO alone (Figure 2E; supplemental Figure 2E), demonstrating a long-term functional deficit in *Tet2; Ncoa4* double KO compared with *Tet2* KO HSPCs.

We hypothesized that acute loss of Ncoa4, without developmental compensation, would more closely reflect the findings from the CRISPR-Cas9 screen. Therefore, we used a Cre recombinase under the Mx promoter (Mx-Cre), which results in the deletion of *Tet2*, *Ncoa4*, or both after injections of polyinosinic:polycytidylic acid. In a transplantation experiment, BM from WT, *Tet2* KO, *Ncoa4* KO, or *Tet2* KO; *Ncoa4* KO was competed against WT in a 20:80 ratio (Figure 2F). After excision of Ncoa4, *Tet2* KO peripheral blood chimerism was significantly reduced compared with Tet2 KO alone in both myeloid and lymphoid fractions (Figure 2G). Consistent with this observation, this reduction in *Tet2;Ncoa4* double KO compared with *Tet2* KO was seen in the lineage negative and HSC fractions of the BM (Figure 2H).

We performed single-cell RNA sequencing (scRNAseq) on sorted LSK HSPCs transduced with either nontargeting (control) or *Ncoa4* gRNAs, to understand the transcriptional effects of *Ncoa4* KO on *Tet2* KO HSPCs. First, we confirmed our observations from the Mx-Cre transgenic, by flow cytometry,[35] that there was a reduction of HSCs ($CD150^+CD48^-CD135^-$LSK) expressing *Ncoa4* gRNA compared with control gRNA (Figure 2I; supplemental Figure 2F). Conversely, *Tet2* KO, but not WT, myeloid-biased multipotent progenitors ($CD150^-CD48^+CD135^-$LSK) increased in number when expressing *Ncoa4* gRNA compared with control gRNA (supplemental Figure 2G). No significant differences in erythroid progenitors were observed in the BM transplantations of WT or *Tet2* KO Cas9 expressing HSCs transduced with *Ncoa4* gRNAs (supplemental Figure 2H-I). Cells expressing *Ncoa4* gRNA exhibited lower *Ncoa4* expression, consistent with CRISPR-Cas9 KO (supplemental Figure 2J). Pseudotime analysis positioned HSCs and progenitor cells along the established differentiation trajectory in both WT and *Tet2* KO HSPCs, with and without *Ncoa4* loss[36,40] (Figure 2J). Consistent with previously reported HSC markers, *Tcf15*-expressing HSCs resided at the earliest pseudotime, followed by cells expressing other HSPC markers such as *Cd34*, *Hlf*, *Flt3*, and *Kit* (supplemental Figure 2K).[41-43] HSPCs further along the pseudotime trajectory expressed surface markers such as *Fcgcr3*,[44] known to be enriched in myeloid progenitors (supplemental Figure 2K). Quantification of cells with early pseudotime signatures revealed that *Ncoa4* loss resulted in a relative decrease in HSCs and a relative increase in progenitor cells, with these effects being more pronounced in *Tet2* KO mice (supplemental Figure 2L-M). Similarly, *Ncoa4* loss in *Tet2* KO HSPCs reduced the expression of stem cell gene signatures to a greater degree than that seen in WT HSPCs (Figure 2K-L; supplemental Figure 2N). In contrast to these differences in differentiation between *Ncoa4* KO and WT cells, there was no increase in apoptosis after CRISPR-Cas9-mediated KO of *Ncoa4* in WT or *Tet2* KO HSCs (supplemental Figure 2O-Q).

In summary, both CRISPR-Cas9 and Cre recombinase-mediated deletion of *Ncoa4* diminished the competitive fitness of *Tet2*-mutant hematopoiesis. Acute depletion of *Ncoa4* by CRISPR-Cas9 or an Mx promoter–driven Cre recombinase reduces HSC numbers in *Tet2*-mutant cells, as observed by flow cytometry and scRNAseq.

Ferritinophagy-dependent labile iron flux is increased in *Tet2* KO HSPCs

Excess intracellular iron is toxic owing to increased oxidative stress (eg, iron-mediated lipid oxidation leading to ferroptosis)[45]; thus, intracellular iron homeostasis is tightly regulated. Excess labile iron ($Fe2^+$) is stored in ferritin and is released in

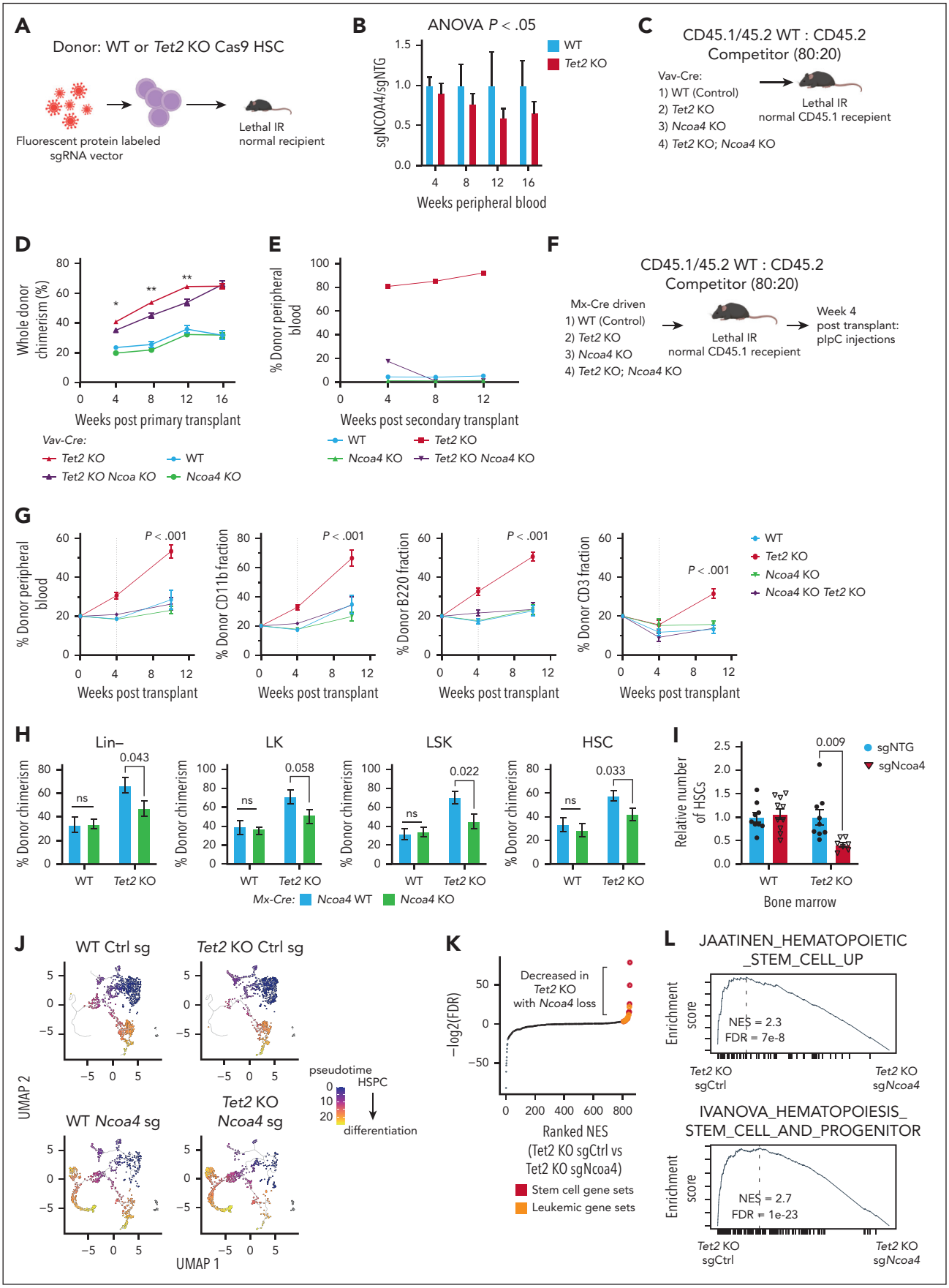
A
Donor: WT or Tet2 KO Cas9 HSC
Fluorescent protein labeled sgRNA vector
Lethal IR normal recipient
B
ANOVA P < .05
WT
Tet2 KO
sgNCOA4/sgNTG
Weeks peripheral blood
C
CD45.1/45.2 WT : CD45.2 Competitor (80:20)
Vav-Cre:
1) WT (Control)
2) Tet2 KO
3) Ncoa4 KO
4) Tet2 KO; Ncoa4 KO
Lethal IR normal CD45.1 recepient
D
Whole donor chimerism (%)
Weeks post primary transplant
Vav-Cre:
Tet2 KO
WT
Tet2 KO Ncoa KO
Ncoa4 KO
E
% Donor peripheral blood
Weeks post secondary transplant
WT
Tet2 KO
Ncoa4 KO
Tet2 KO Ncoa4 KO
F
CD45.1/45.2 WT : CD45.2 Competitor (80:20)
Mx-Cre driven
1) WT (Control)
2) Tet2 KO
3) Ncoa4 KO
4) Tet2 KO; Ncoa4 KO
Lethal IR normal CD45.1 recepient
Week 4 post transplant: pIpC injections
G
% Donor peripheral blood
% Donor CD11b fraction
% Donor B220 fraction
% Donor CD3 fraction
P < .001
Weeks post transplant
WT
Tet2 KO
Ncoa4 KO
Ncoa4 KO Tet2 KO
H
Lin–
LK
LSK
HSC
% Donor chimerism
ns
0.043
0.058
0.022
0.033
WT
Tet2 KO
Mx-Cre: Ncoa4 WT Ncoa4 KO
I
Relative number of HSCs
0.009
sgNTG
sgNcoa4
WT
Tet2 KO
Bone marrow
J
WT Ctrl sg
Tet2 KO Ctrl sg
WT Ncoa4 sg
Tet2 KO Ncoa4 sg
UMAP 2
UMAP 1
pseudotime
HSPC
differentiation
K
−log2(FDR)
Decreased in Tet2 KO with Ncoa4 loss
Ranked NES (Tet2 KO sgCtrl vs Tet2 KO sgNcoa4)
Stem cell gene sets
Leukemic gene sets
L
JAATINEN_HEMATOPOIETIC_STEM_CELL_UP
Enrichment score
NES = 2.3
FDR = 7e-8
Tet2 KO sgCtrl
Tet2 KO sgNcoa4
IVANOVA_HEMATOPOIESIS_STEM_CELL_AND_PROGENITOR
NES = 2.7
FDR = 1e-23

Figure 2.

response to cellular demands by lysosomal degradation of ferritin,[46] a process known as ferritinophagy. NCOA4 is an adapter for ferritin heavy chain (FTH1), directing FTH1 to autophagosomes resulting in the release of labile iron ($Fe2^+$) after lysosomal degradation of their contents.[46,47] The selective reliance of *Tet2* KO HSPCs on *Ncoa4* suggests that the *Tet2* KO cells have a greater requirement for labile iron. To test this hypothesis, we examined whether iron availability selectively affects *Tet2* KO cell growth compared with WT cells. To examine this question in vitro, we used *Tet2* KO and WT HSPCs immortalized by exogenous expression of a *Hoxb8-ER* fusion.[48] We found that the selective growth advantage of *Tet2* KO Hoxb8-ER relative to WT cells was dependent on abundant iron availability in the media (Figure 3A).

Based on the selective dependency of *Tet2* KO cells on *Ncoa4* and iron availability, we hypothesized that *Tet2* KO cells have increased ferritinophagy to maintain labile iron availability. We assessed ferritinophagy by measuring FTH1 protein levels, including the lysosome-processed FTH1 product, at steady state and in response to either activators or inhibitors of ferritin degradation (iron chelation or lysosomal protease inhibitors, respectively) (Figure 3B). As expected, the lysosomal cathepsin inhibitor E64D decreased the lysosome-processed FTH1 product,[47] both at steady state and after FTH1 degradation stimulated by iron chelation (deferoxamine) (Figure 3B; supplemental Figure 3A). We found an increase in the lysosome-degraded form of FTH1, consistent with a higher level of ferritinophagy in *Tet2* KO *Hoxb8-ER* HSPCs than WT cells (Figure 3B).

An increase in lysosomal degradation of FTH1 should result in greater labile iron ($Fe2^+$) release.[49] To test this, we isolated primary WT and *Tet2* KO HSCs and used an intracellular dye to measure labile iron concentration, with or without deferoxamine treatment to control for the dye specificity. We observed in primary *Tet2* KO HSCs and HSPCs an increase in intracellular labile iron compared with WT, which was dependent on iron chelation (Figure 3C; supplemental Figure 3B). To confirm that intracellular ferritinophagy via *Ncoa4* is a major source of labile iron in *Tet2* KO, we knocked down *Ncoa4* using short hairpin RNA, which reduced lysosomal degradation of FTH1 and labile iron pool (supplemental Figure 3C-E).[49] Recovery of HSC expansion and peripheral blood chimerism by week 16 in our Vav-Cre-dependent *Ncoa4* KO system, which results in fetal hematopoietic KO of both *Tet2* and *Ncoa4* (Figure 2C-D),[50,51] was associated with an increased expression of the transferrin receptor (CD71) in HSCs and HSPCs (supplemental Figure 2C-D). This suggested increased iron uptake followed *Ncoa4* KO to maintain the labile iron demand in *Tet2* KO HSPCs.

After ferritin degradation, intracellular iron is released from lysosomes. We sought to manipulate labile iron release from lysosomes in vivo to investigate whether this mimics the effects of *Ncoa4* KO on *Tet2*-mutant hematopoiesis. Lysosomal iron release can be inhibited with ironomycin, which sequesters iron in lysosomes both in vitro and in vivo[52] (supplemental Figure 3F-G). To investigate whether ironomycin has a greater effect on *Tet2* KO HSPCs than WT, we competitively transplanted *Tet2* KO and WT BM at a 20:80 ratio into lethally irradiated recipient mice and monitored engraftment. After engraftment, recipient mice were treated with a 4-week intraperitoneal course of ironomycin (3 mg/kg) or vehicle control[53] (Figure 3D). Inhibition of lysosomal iron release by ironomycin reduced *Tet2* KO expansion in myeloid but not lymphoid compartments (Figure 3E; supplemental Figure 3H-I), consistent with results from our *Tet2; Ncoa4* double KO Vav-Cre system. *Tet2* KO LSK HSPC chimerism decreased in mice treated with ironomycin compared with control (Figure 3F).

These experiments demonstrate that the increased cell growth of *Tet2* KO relative to WT cells is dependent on iron availability. *Ncoa4* regulates intracellular labile iron, depletion of iron decreases the competitive growth of *Tet2* KO cells, and *Tet2* KO HSPCs have elevated iron levels and increased ferritinophagy compared with WT cells. Pharmacologic inhibition of lysosomal iron release, an alternative mechanism to decrease labile iron availability, phenocopied loss of *Ncoa4*, decreasing the competitive advantage of *Tet2* KO HSPCs.

Figure 2. *Ncoa4* KO impairs *Tet2* KO competitive advantage in mouse transplant models. (A) Competitive transplantation of Cas9 expressing WT or *Tet2* KO HSCs ($CD150^+CD135^-CD48^-$lineage$^-Sca1^+Kit^+$) transduced with sgRNA targeting *Ncoa4* (sgNcoa4) or sgRNA nontargeting control (sgNTG). Lentiviral vector expresses a fluorescent protein, enabling tracing of transduced hematopoietic progeny. (B) Serial peripheral blood flow cytometric analysis after transplantation of WT or *Tet2* KO cells containing blue fluorescent protein–labeled sgNTG or red fluorescent protein–labeled sgNcoa4. Results were normalized to the percentage of blue fluorescent protein–labeled cells expressing sgNTG. Significance test by 2-way ANOVA. Bars showing mean with standard error of the mean (SEM). N = 9 to 10 mice per arm. (C) Competition experiment between Vav-Cre^+;Cd45.1/2 control cells and either *Tet2* fl/fl Vav-Cre^+;Cd45.2 (*Tet2* KO), *Ncoa4* fl/fl Vav-Cre^+;Cd45.2 (*Ncoa4* KO), *Tet2* fl/fl *Ncoa4* fl/fl Vav-Cre^+Cd45.2 (*Tet2* KO *Ncoa4* KO), or WT Vav-Cre^+;Cd45.2 BM cells transplanted at an 80:20 (WT-to-competitor) ratio, injected into lethally IR Cd45.1 recipients. (D) CD45.2 chimerism analysis from peripheral blood at each time point, as a percentage of total donor (CD45.2 and CD45.1/CD45.2) in mice transplanted with Vav-Cre transgenic mice as per panel C. Bars showing mean with SEM. N = 18 to 20 mice per arm. Unpaired *t* test between *Tet2* KO and *Tet2* KO *Ncoa4* KO. $*P < .01$; $**P < .001$. (E) Transplant of whole BM from primary Vav-Cre transgenic mice (from panel C) into secondary recipients. Peripheral blood analysis of whole BM based on CD45 chimerism. Bars showing mean with SEM. N = 5 mice per arm. (F) Competition experiment between Mx-Cre^+;Cd45.1/2 control and either *Tet2* fl/fl Mx-Cre^+;Cd45.2 (*Tet2* KO), *Ncoa4* fl/fl Mx-Cre^+;Cd45.2 (*Ncoa4* KO), *Tet2* fl/fl *Ncoa4* fl/fl Mx-Cre^+Cd45.2 (*Tet2* KO *Ncoa4* KO), or WT Mx-Cre^+;Cd45.2 BM cells. BM transplanted at an 80:20 (WT-to-competitor) ratio into lethally IR Cd45.1 recipients. pIpC injections 10 mg/kg intraperitoneally on alternate days for 3 doses. (G) CD45.2 chimerism analysis from peripheral blood at each time point, as a percentage of total donor (CD45.2 and CD45.1/CD45.2) from panel F. Bars showing mean with SEM. N = 17 to 20 mice per arm. Unpaired *t* test between *Tet2* fl/fl and *Tet2* fl/fl*; Ncoa4* fl/fl. Dashed line demarcates the start of pIpC injections. (H) CD45 chimerism in lineage negative, LK, LSK, and $CD150^+CD48^-$LSK (HSC) BM fractions from Mx-Cre transgenic mice from panel F at 11 weeks after transplant. N = 9 to 10 mice per arm. Unpaired *t* test between genotypes indicated. (I) Flow cytometric analysis of HSC and multipotent progenitor BM populations from mice transplanted with Cas9-expressing WT or *Tet2* KO HSCs infected with either sgNcoa4 or sgNTG. Results were normalized to the percentage of cells expressing sgNTG. The flow gating strategy is depicted in supplemental Figure 2F. Unpaired *t* test, bars showing mean with SEM. Each point represents an individual mouse. N = 7 to 10 mice per arm. (J) Pseudotime trajectory of WT or *Tet2* KO Cas9 LSK HSPCs transduced with control or *Ncoa4* gRNAs. Analysis was performed using Monocle3.[36] Pseudotime trajectory annotation with expression of stem and HSPC markers is highlighted in supplemental Figure 2K. (K) Using cell clusters at the top of the pseudotime trajectory (blue label), which excludes differentiated Fcgcr3+ progenitors, gene set enrichment analysis was performed using all of the C2 Molecular Signatures Database.[37] *Tet2* KO HSPCs transduced with control nontargeting gRNAs were compared with *Tet2* KO HSPCs transduced with *Ncoa4* gRNAs (gNcoa4). This revealed enrichment of gene sets expressed in stem cell (red) and leukemia (orange) signatures. (L) Highlighted HSPC gene sets enriched in sgNTG compared with sgNcoa4 transduced *Tet2* KO HSPCs. ANOVA, analysis of variance; IR, irradiated; LK, lineage$^-$cKit$^+$; pIpC, polyinosinic:polycytidylic acid.

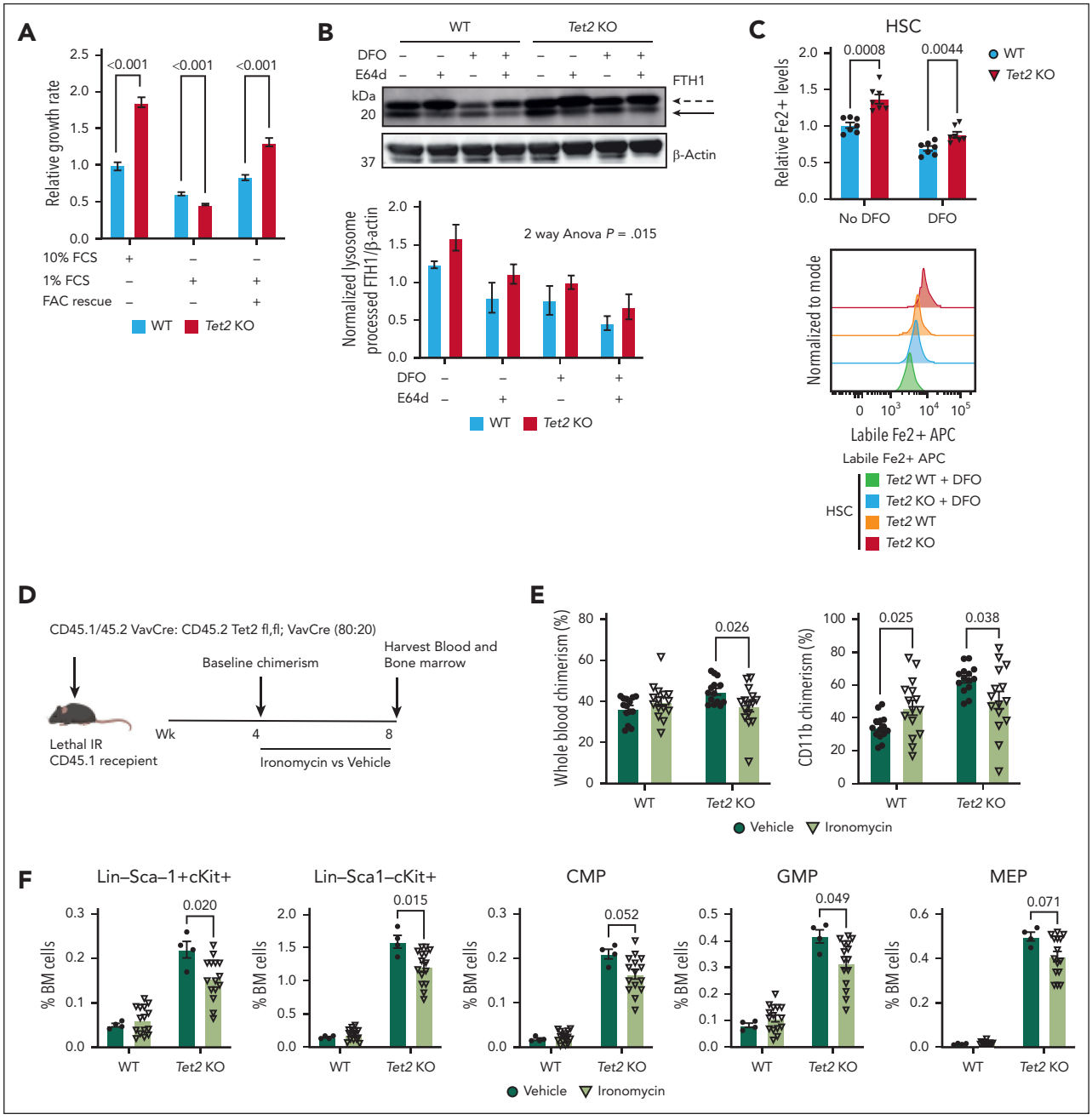

Figure 3. Expansion of *Tet2* KO HSPCs is dependent on lysosome-dependent ferritinophagy. (A) *Tet2* fl/fl; Vav-Cre$^+$ (*Tet2* KO) compared with Vav-Cre$^+$ (WT) Hoxb8-ER immortalized HSPC have increased growth after 4 days in RPMI + 10% FCS, but not in 1% FCS unless supplemented with FAC (100 μM). N = 6. (B) Immunoblot of WT and *Tet2* KO Hoxb8-ER HSPC treated with DFO 50 μM and/or E64D lysosomal protease inhibitor 2 μg/mL for 16 hours. Immunoblot with FTH1 and β-actin antibody. Dashed line, total FTH1 protein; solid line, lysosomal degraded FTH1 product.[47] Fold-change quantification of lysosomal degraded FTH1 product, normalized to β-actin and untreated WT cells. N = 3. (C) Cytoplasmic $Fe2^+$ pool in HSC from *Tet2* KO compared with WT. Median fluorescent intensity of labile iron stain relative to untreated WT. Cells were treated with either DFO at 50 μM or vehicle control during concurrent staining to demonstrate the specificity of the labile iron stain. Each dot represents an individual mouse. Gating strategy as per supplemental Figure 2F. Representative flow cytometry histogram of HSCs from WT or *Tet2* KO mice. N = 7. (D) Schematic of a competition experiment between WT or *Tet2* KO CD45.2$^+$ (20% composition) and WT CD45.1$^+$/CD45.2$^+$ control (80% composition) BM cells transplanted into lethally IR CD45.1 recipients. After engraftment at 4 weeks, mice were treated with a 4-week treatment of ironomycin (3 mg/kg intraperitoneally 5 days/wk) vs vehicle before harvest for peripheral blood and BM. (E) Peripheral blood analysis of whole blood and CD11b compartments and (F) BM analysis of CD45.2$^+$ *Tet2* KO and CD45.1$^+$/CD45.2$^+$ WT donor chimerism after a 4-week treatment of either ironomycin or vehicle control. Each point represents an individual mouse. N = 12 to 15 per arm. Bars show mean with SEM, with unpaired *t* test used unless otherwise specified. CMP, common myeloid progenitor; DFO, deferoxamine; FAC, ferric ammonium citrate; FCS, fetal calf serum; GMP, granulocyte-monocyte progenitor; IR, irradiated; MEP, megakaryocyte-erythroid progenitor.

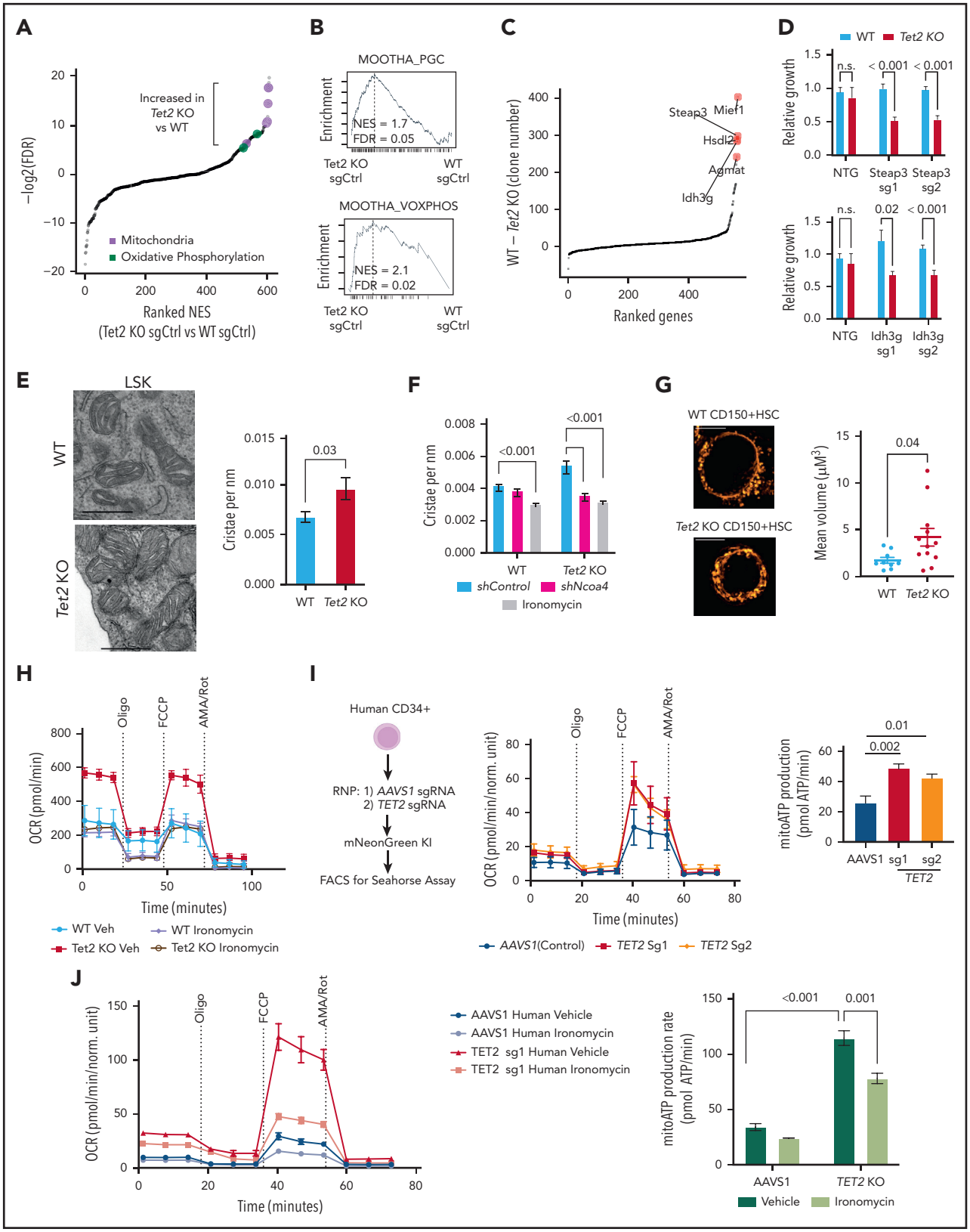

Figure 4. Increased mitochondrial ATP production in *Tet2* KO HSPCs is dependent on ferritinophagy. (A) Using cell clusters at the top of the pseudotime trajectory (blue label) (from Figure 2J), which excludes Fcgcr3^{+} differentiated progenitors, gene set enrichment analysis was performed comparing WT with *Tet2* KO HSPCs using all of the C2 Molecular Signatures Database.[37] This revealed enrichment of gene sets involved in mitochondrial function (purple) and oxidative phosphorylation (green). (B) Highlighted mitochondrial and oxidative phosphorylation gene sets comparing WT with *Tet2* KO HSPCs. (C) Targeted CRISPR screen using mitochondrial and iron homeostasis regulatory genes in WT and *Tet2* KO Cas9 LSK HSPCs. *Tet2* KO HSPCs exhibit genetic dependency on regulators of iron, mitochondrial respiration, and translation. Highlighted genes have a false discovery rate of <0.25, WT/Tet2 KO persisting clone differences of >2, and WT/Tet2 KO VAF of >1. (D) Doxycycline-inducible Cas9 expressing WT or Tet2 fl/fl

Ferritinophagy maintains increased mitochondrial adenosine triphosphate (ATP) production in *Tet2* KO compared with WT HSPCs

We next sought to identify specific cellular processes that increase iron demand in *Tet2* KO HSPCs compared with WT. We compared scRNAseq results between WT and *Tet2* KO LSKs transduced with control sgRNA for hematopoietic cells at similar differentiation states in the earliest pseudotime clusters. Gene set enrichment analysis in *Tet2* KO vs WT HSCs revealed increased expression of oxidative phosphorylation, mitochondrial, and *PGC-1alpha* gene sets (Figure 4A-B).[54]

To complement the analysis of gene sets enriched in *Tet2* KO cells, we performed an in vivo genetic screen using our UMI-labeled CRISPR-Cas9 screening platform with a curated library of 4440 sgRNAs targeting 1032 genes related to iron homeostasis and mitochondrial function. The screen highlighted *Steap3*, a ferrireductase that converts $Fe3^+$ to labile $Fe2^+$, as one of the top dependencies for *Tet2* KO expansion (Figure 4C-D; supplemental Figure 4A). In addition, genes involved in mitochondrial respiration (*Idh3g*) and mitochondrial translation (*Mief1*) were selectively required for the clonal advantage of *Tet2* KO relative to WT cells (Figure 4C-D). These findings provide further evidence that *Tet2* KO clonal fitness is selectively dependent on labile iron homeostasis and mitochondrial function.[55]

Given the selective dependence of *Tet2* KO HSPCs on mitochondrial synthesis and function, we hypothesized that *Tet2* KO and WT HSPCs might exhibit differences in mitochondrial morphology. Using transmission electron microscopy, we examined mitochondrial features in WT and *Tet2* KO LSK HSPCs, specifically focusing on mitochondrial cristae morphology. Cristae, the location of the respiratory electron transport chain, adapt to meet the cell's metabolic demands, and these morphologic adaptations define cellular respiratory capacity.[56-60] Indicative of increased mitochondrial respiration, *Tet2* KO HSPCs and Hoxb8-ER cells had higher cristae density than that of WT (Figure 4E-F; supplemental Figure 4B). Given that the competitive advantage of *Tet2* KO HSPCs is iron dependent, we investigated whether cristae density in *Tet2* KO Hoxb8-ER cells could be reversed by inhibiting ferritinophagy. Both *Ncoa4* short hairpin RNA knockdown and ironomycin treatment reduced the cristae density of *Tet2* KO Hoxb8-ER cells to that of WT cells (Figure 4F; supplemental Figure 4B).

To determine whether this mitochondrial difference seen in HSPCs extends to HSCs ($CD135^-CD34^-CD48^-CD150^+$LSK), we stained mitochondria in WT and *Tet2* KO HSCs. Three-dimensional structured illumination microscopy images were analyzed via a validated pipeline,[61-63] demonstrating that *Tet2* KO HSCs have increased mitochondrial volume compared with WT (Figure 4G). Finally, quantitative polymerase chain reaction measurement of mitochondrial DNA suggested increased mitochondrial mass in *Tet2* KO compared with WT Hoxb8-ER cells (supplemental Figure 4C).[64]

To assess whether these phenotypic changes corresponded to functional increases in mitochondrial ATP production, we performed Seahorse Mito Stress assays. Mitochondrial ATP production in *Tet2* KO Hoxb8 HSPCs was markedly increased compared with WT. Once again, this could be reversed with *Ncoa4* knockdown or ironomycin treatment (Figure 4H; supplemental Figure 4D-E). This finding demonstrates that mitochondrial ATP production, in addition to mitochondrial cristae density, is increased in *Tet2* KO cells.

We next sought to determine whether the increase in mitochondrial ATP production observed in *Tet2* KO HSPCs is conserved in human HSPCs. Using human umbilical cord blood $CD34^+$ HSPCs, we edited the genomic loci at either *TET2* or control site (*AAVS1*) using a Cas9-ribonucleotide protein sgRNA complex. To mark $CD34^+$ HSPCs with successful *TET2* editing, an adenovirus vector encoding a fluorescent reporter (mNeonGreen) and a sequence with homology to the edited genomic sites was introduced. This allowed integration of the gene encoding a fluorescent protein at the CRISPR-edited site via homologous recombination.[65] We performed the Seahorse Mito Stress assay on the purified, successfully edited control or *TET2*-mutated HSPCs. Consistent with the findings in murine cells, human $CD34^+$ cells with an edited *TET2* locus had an elevated mitochondrial ATP production rate (Figure 4I; supplemental Figure F). Inhibition of ferritinophagy using ironomycin reduced the increase in mitochondrial ATP production seen in *TET2*-mutant human $CD34^+$ cord blood cells (Figure 4J).

In summary, in *Tet2* KO HSPCs, we observed increased mitochondria cristae density and mass correlating with a ferritinophagy-dependent increase in mitochondrial ATP production. We note that this ferritinophagy-dependent increase in mitochondrial ATP production was also conserved in human $CD34^+$ HSPCs with *TET2* mutations.

Discussion

We used a large-scale barcoded CRISPR/Cas9 screening platform to perform clonally tracked genetic perturbations in HSPCs

Figure 4 (continued) Vav1-Cre (Tet2 KO) in Hoxb8 HSPC system transduced with either control sgRNA (NTG) or *Steap3* targeting sgRNA (sg1 and sg2) or *Idh3g* targeting sgRNA (sg1 and sg2). Growth relative to no doxycycline-treated cells at 4 days. N = 5. Bars showing mean ± SEM, unpaired *t* test. (E) Transmission electron microscopy (TEM) of primary WT and *Tet2* KO LSK HSPCs. Cristae number normalized to the length of mitochondria. Scale bar, 500 nm. N = 50 to 57 mitochondria from 5 mice per genotype. Mean and SEM are displayed with results of unpaired *t* test. (F) TEM of WT and *Tet2* KO Hoxb8 with control short hairpin RNA (shRNA), *Ncoa4* shRNA, or ironomycin treatment 50 nM for 48 hours. Images in supplemental Figure 4B. Cristae number was normalized to the length of mitochondria. N = 30 to 71 mitochondria per experimental condition. Mean and SEM are displayed with results of unpaired *t* test. (G) Mitochondrial staining of primary WT and *Tet2* KO $CD135^-CD48^-CD34^-CD150^+$ HSCs. Scale bar, 5 μm. Representative slice from a 3-dimensional structured illumination microscopy image shown. Quantification of mean volume divided by counted mitochondria. Bars showing mean ± SEM, with unpaired *t* test. Each dot represents an analysis of an individual cell from 5 mice per genotype. (H) Representative Seahorse Mito Stress assay of WT and *Tet2* KO Hoxb8-ER cells treated with either vehicle (dimethyl sulfoxide [DMSO]) or ironomycin (50 nM) for 48 hours. Quantification of mitochondrial and glycolytic ATP production is shown in supplemental Figure 4D. (I) Primary human $CD34^+$ umbilical cord HSPCs were transfected with either *AAVS1* or *TET2* (sg1 and sg2) gRNA–CRISPR-Cas9 RNP complexes. Adenovirus encoding mNeonGreen sequence with adjoining DNA sequence homologous to edited loci results in integration at targeted genes. Fluorescent activated cell sorting (FACS) was used to purify successfully edited cells identified via mNeonGreen expression. Purified cells were analyzed with the Seahorse Mito Stress assay. The mitochondrial ATP production rate is derived from OCR and extracellular acidification rate. N = 7. (J) Seahorse Mito Stress assay on primary human CD34 HSPCs transfected with either *AAVS1* or *TET2* targeting gRNA were treated with either DMSO (vehicle) or ironomycin 200 nM for 48 hours. Quantification of mitochondrial ATP production was summarized from Seahorse assays. N = 2-6. Mean and SEM are displayed with results of unpaired *t* test. AMA/Rot, antimycin A/rotenone; FCCP, carbonyl cyanide-p-trifluoromethoxyphenylhydrazone; KI, knockin; OCR, oxygen consumption rate; Oligo, oligomycin; RNP, ribonucleoprotein.

over long-term transplantation, thereby identifying selective dependencies of *Tet2* KO HSPCs. We identified *Ncoa4* as a vulnerability in our model of *Tet2*-deficient CHIP. NCOA4 is an adapter protein that directs ferritin to lysosomes, resulting in autophagy-dependent degradation (ferritinophagy). Our data suggest that *Tet2* KO HSPCs have increased ferritinophagic flux and an expanded labile iron ($Fe2^+$) pool, which is acutely inhibited by *Ncoa4* knockdown. Through microscopy, genetic perturbations, and mitochondrial assays, we demonstrate that *Tet2*-deficient HSPCs have increased mitochondrial demand in comparison to WT and that reducing ferritinophagic flux and labile iron content, through either *Ncoa4* knockdown or ironomycin treatment, reduces mitochondrial ATP production in *Tet2* KO cells.

Using nucleotide-based UMIs, we were able to track stem and progenitor cells clonally in a large-scale in vivo CRISPR/Cas9 KO screen. Our screens demonstrate the capability of this strategy to study stem and progenitor cell biology, which requires long-term tracking of clonal dynamics. For example, by conventional analysis, HSPCs with genetic perturbations against known cancer genetic drivers (eg, *Dnmt3a*) are mistakenly identified as deleterious to stem and progenitor cell function because they increase stem cell renewal[66] and reduce proliferation during hematopoietic differentiation (supplemental Table 3). The tracking of clonal growth over long-term transplantation using barcodes enables the identification of true genetic dependencies by tracking malignant clones with late clonal growth. Other putative targets requiring further validation may provide novel insights into *Tet2*-mutant HSPC biology (supplemental Table 2). Our ability to identify an important regulator of iron homeostasis as a dependency in HSPCs was contingent on performing this screen in vivo, where local iron availability in the HSC niche is dependent on BM macrophages.[67] Previous CRISPR-Cas9 screens in primary HSPCs have been predominantly limited to in vitro settings[68] or to smaller sgRNA libraries.[41] Recent work, which is complementary to our approach, has used an in vivo CRISPR-Cas9 screen to assess genetic perturbations and single-cell transcriptomics simultaneously.[69] Efforts to understand clonal dynamics using nucleotide barcoded CRISPR-Cas9 screen in vivo have been applied to more differentiated cells such as T cells.[70] The ability to track clonal growth in vivo has many potential applications including tracking clonal infiltration into tumors and tissues and studying normal and malignant cell biology in a physiologic setting.

We identified labile iron ($Fe2^+$) as a dependency for the competitive advantage of *Tet2* KO HSPCs, which exhibit increased HSC self-renewal[5] and clonal expansion in CHIP.[2] The importance of iron availability in maintaining HSCs has been recently recognized.[67,71] *Ncoa4* plays a central role in maintaining this iron dependency by mediating ferritinophagy, the autophagy-dependent degradation of ferritin that releases $Fe2^+$. We confirmed that inhibition of ferritinophagy, genetically, by *Ncoa4* KO, or pharmacologically, with ironomycin reduced *Tet2* KO HSC numbers relative to WT HSCs. Our observations that reducing iron availability through *Ncoa4* inhibition reverses the mitochondrial phenotype seen in *Tet2* KO cells are consistent with a previous study in pancreatic cancer showing that *NCOA4* knockdown downregulates mitochondrial iron-sulfur cluster-containing proteins, which are important for the electron transport chain and mitochondrial respiration.[49] The dependency on ferritinophagy observed in *Tet2*-mutant CHIP in our study and in recent work in primary human AML stem cells[72] suggests that ferritinophagy is a dependency across myeloid malignancies. Although iron overload is commonly observed in MDS, *Ncoa4* is overexpressed in BM stem and progenitor cells from patients with MDS compared with healthy individuals,[73] highlighting a persistent demand for labile iron, and iron chelation seems to improve event-free survival in individuals with MDS.[74] Agents that inhibit NCOA4 activity are in development for clinical use.[75]

A striking finding of this study is the difference in mitochondrial morphology and function between *Tet2* KO and WT HSPCs. *Tet2* KO HSPCs exhibit increased mitochondrial size and cristae density compared with WT. Experimental evidence suggests that inhibiting mitochondrial fusion is sufficient to decrease cellular proliferation,[76] indicating a possible link between *Tet2* KO clonal outgrowth and its mitochondrial morphology. Our functional findings are consistent with the observation of increased oxidative phosphorylation gene expression program in HSCs from patients with *TET2*-mutated CHIP compared with healthy individuals.[77]

In summary, we identified genetic dependencies of *Tet2* KO stem and progenitor cells using a large UMI-barcoded CRISPR-Cas9 in vivo screen. We describe an important role for *Ncoa4*-mediated ferritinophagy, linked to increased iron utilization for mitochondrial ATP metabolism in stem cells, as a mechanism that aids clonal advantage in CHIP and myeloid malignancies.

Acknowledgments

The authors are grateful to Vamsi Mootha and Jordan Wengrod for their helpful discussions. Electron microscopy imaging, consultation, and services were performed in the Harvard Medical School Electron Microscopy Facility. Microscopy Resources on the North Quad Core at Harvard Medical School provided 3-dimensional imaging.

J.L. is a recipient of a Cancer Research UK–American Association for Cancer Research Transatlantic Fellowship. B.L.E. received support for this work from National Heart, Lung, and Blood Institute, National Institutes of Health (NIH) grant R01HL082945, National Cancer Institute (NCI), NIH grants P01CA066996 and R35CA253125, the Howard Hughes Medical Institute, the Edward P. Evans Foundation, and the Adelson Medical Research Foundation. P.G.K. is a recipient of the Burroughs Wellcome Fund Career Awards for Medical Scientists and a Damon Runyon Physician-Scientist Training Award supported by the Damon Runyon Cancer Research Foundation (PST-35-21) and received support from the Edward P. Evans Foundation for partial support of this work. C.B.H. received support from NCI, NIH grant T32-CA251062, the Edward P. Evans Foundation, the Academy of Clinical Laboratory Physicians and Scientists, and the Pan-Mass Challenge FLAMES team. S.A.A. is supported by NCI, NIH grant CA066996.

Authorship

Contribution: J.L., P.G.K., and B.L.E. designed the study and wrote the manuscript; J.L., P.G.K., T.T.P.N., M.B., M.M., A.M., W.S., C.B.H., M.E., A.N., and P.M.L. performed and analyzed experiments; S.A.A. and J.D.M. contributed research tools and helped design the study; and all authors reviewed and edited the manuscript.

Conflict-of-interest disclosure: B.L.E. has received research funding from Novartis and Calico; has received consulting fees from AbbVie; and is a

member of the scientific advisory board and a shareholder for Neomorph Inc, Big Sur Bio, Skyhawk Therapeutics, and Exo Therapeutics. C.B.H. has received consulting fees from 48 Bio. S.A.A. has been a consultant and/or shareholder for Neomorph Inc, C4 Therapeutics, Hyku Therapeutics, Stelexis Therapeutics, and Nimbus Therapeutics; has received research support from Janssen and Syndax; and is an inventor on a patent related to menin inhibition (WO/2017/132398A1). J.D.M. is an inventor on a patent related to targeting ferritinophagy (WO/2015/149006A3); reports research support from Novartis and Casma Therapeutics; and has consulted for Third Rock Ventures and Skyhawk Therapeutics, all unrelated to the submitted work. J.L. has received consulting fees from TScan and Jazz Pharmaceuticals. The remaining authors declare no competing financial interests.

ORCID profiles: J.L., 0000-0002-0725-069X; P.G.K., 0000-0002-8716-8759; T.T.P.N., 0000-0002-3507-2309; B.L.E., 0000-0003-0197-5451.

Correspondence: Benjamin L. Ebert, Department of Medical Oncology, Dana-Farber Cancer Institute, 450 Brookline Ave, Boston, MA 02115; email: benjamin_ebert@dfci.harvard.edu.

Footnotes

Submitted 13 December 2024; accepted 6 May 2025; prepublished online on *Blood* First Edition 10 June 2025. https://doi.org/10.1182/blood.2024028033.

*J.L. and P.G.K. contributed equally to this study.

Single-cell RNA sequencing data have been deposited in the Gene Expression Omnibus database (accession number GSE289732).

For any additional data inquiries, please contact the corresponding author, Benjamin L. Ebert (benjamin_ebert@dfci.harvard.edu).

The online version of this article contains a data supplement.

There is a *Blood* Commentary on this article in this issue.

The publication costs of this article were defrayed in part by page charge payment. Therefore, and solely to indicate this fact, this article is hereby marked "advertisement" in accordance with 18 USC section 1734.

REFERENCES

1. Jaiswal S, Fontanillas P, Flannick J, et al. Age-related clonal hematopoiesis associated with adverse outcomes. *N Engl J Med*. 2014;371(26):2488-2498.
2. Fabre MA, de Almeida JG, Fiorillo E, et al. The longitudinal dynamics and natural history of clonal haematopoiesis. *Nature*. 2022;606(7913):335-342.
3. Lee-Six H, Øbro NF, Shepherd MS, et al. Population dynamics of normal human blood inferred from somatic mutations. *Nature*. 2018;561(7724):473-478.
4. Ito S, D'Alessio AC, Taranova OV, Hong K, Sowers LC, Zhang Y. Role of Tet proteins in 5mC to 5hmC conversion, ES-cell self-renewal and inner cell mass specification. *Nature*. 2010;466(7310):1129-1133.
5. Moran-Crusio K, Reavie L, Shih A, et al. Tet2 loss leads to increased hematopoietic stem cell self-renewal and myeloid transformation. *Cancer Cell*. 2011;20(1):11-24.
6. Delhommeau F, Dupont S, Valle VD, et al. Mutation in TET2 in myeloid cancers. *N Engl J Med*. 2009;360(22):2289-2301.
7. Comazzetto S, Shen B, Morrison SJ. Niches that regulate stem cells and hematopoiesis in adult bone marrow. *Dev Cell*. 2021;56(13):1848-1860.
8. Ding L, Morrison SJ. Haematopoietic stem cells and early lymphoid progenitors occupy distinct bone marrow niches. *Nature*. 2013;495(7440):231-235.
9. Decker M, Leslie J, Liu Q, Ding L. Hepatic thrombopoietin is required for bone marrow hematopoietic stem cell maintenance. *Science*. 2018;360(6384):106-110.
10. Mantel CR, O'Leary HA, Chitteti BR, et al. Enhancing hematopoietic stem cell transplantation efficacy by mitigating oxygen shock. *Cell*. 2015;161(7):1553-1565.
11. Ramdas B, Mali RS, Palam LR, et al. Driver mutations in leukemia promote disease pathogenesis through a combination of cell-autonomous and Niche modulation. *Stem Cell Rep*. 2020;15(1):95-109.
12. Mistry JJ, Young KA, Colom Díaz PA, Maestre IF, Levine RL, Trowbridge JJ. Mesenchymal stromal cell senescence induced by Dnmt3a -mutant hematopoietic cells is a targetable mechanism driving clonal hematopoiesis and initiation of hematologic malignancy. *bioRxiv*. Preprint posted online 9 November 2023. https://doi.org/10.1101/2023.11.09.566361
13. McClatchy J, Strogantsev R, Wolfe E, et al. Clonal hematopoiesis related TET2 loss-of-function impedes IL1β-mediated epigenetic reprogramming in hematopoietic stem and progenitor cells. *Nat Commun*. 2023;14(1):8102.
14. Weinreb C, Rodriguez-Fraticelli A, Camargo FD, Klein AM. Lineage tracing on transcriptional landscapes links state to fate during differentiation. *Science*. 2020;367(6479):eaaw3381.
15. Naik SH, Perié L, Swart E, et al. Diverse and heritable lineage imprinting of early haematopoietic progenitors. *Nature*. 2013;496(7444):229-232.
16. Lu R, Neff NF, Quake SR, Weissman IL. Tracking single hematopoietic stem cells in vivo using high-throughput sequencing in conjunction with viral genetic barcoding. *Nat Biotechnol*. 2011;29(10):928-933.
17. Morita Y, Ema H, Nakauchi H. Heterogeneity and hierarchy within the most primitive hematopoietic stem cell compartment. *J Exp Med*. 2010;207(6):1173-1182.
18. Busch K, Klapproth K, Barile M, et al. Fundamental properties of unperturbed haematopoiesis from stem cells in vivo. *Nature*. 2015;518(7540):542-546.
19. Datlinger P, Rendeiro AF, Schmidl C, et al. Pooled CRISPR screening with single-cell transcriptome readout. *Nat Methods*. 2017;14(3):297-301.
20. Griffin GK, Wu J, Iracheta-Vellve A, et al. Epigenetic silencing by SETDB1 suppresses tumour intrinsic immunogenicity. *Nature*. 2021;595(7866):309-314.
21. Kanamori M, Konno H, Osato N, Kawai J, Hayashizaki Y, Suzuki H. A genome-wide and nonredundant mouse transcription factor database. *Biochem Biophys Res Commun*. 2004;322(3):787-793.
22. Meier JA, Zhang F, Sanjana NE. GUIDES: sgRNA design for loss-of-function screens. *Nat Methods*. 2017;14(9):831-832.
23. Wilkinson AC, Ishida R, Kikuchi M, et al. Long-term ex vivo haematopoietic-stem-cell expansion allows nonconditioned transplantation. *Nature*. 2019;571(7763):117-121.
24. Kühn R, Schwenk F, Aguet M, Rajewsky K. Inducible gene targeting in mice. *Science*. 1995;269(5229):1427-1429.
25. Malcovati L, Papaemmanuil E, Ambaglio I, et al. Driver somatic mutations identify distinct disease entities within myeloid neoplasms with myelodysplasia. *Blood*. 2014;124(9):1513-1521.
26. Tara S, Isshiki Y, Nakajima-Takagi Y, et al. *Bcor* insufficiency promotes initiation and progression of myelodysplastic syndrome. *Blood*. 2018;132(23):2470-2483.
27. Shrestha R, Sakata-Yanagimoto M, Maie K, et al. Molecular pathogenesis of progression to myeloid leukemia from TET-insufficient status. *Blood Adv*. 2020;4(5):845-854.
28. Schmidt CR, Achille NJ, Kuntimaddi A, et al. BCOR binding to MLL-AF9 is essential for leukemia via altered EYA1, SIX, and MYC activity. *Blood Cancer Discov*. 2020;1(2):162-177.
29. Vu T, Straube J, Porter AH, et al. Hematopoietic stem and progenitor cell-restricted Cdx2 expression induces transformation to myelodysplasia and acute leukemia. *Nat Commun*. 2020;11(1):3021.

30. Bamezai S, Pulikkottil AJ, Yadav T, et al. A noncanonical enzymatic function of PIWIL4 maintains genomic integrity and leukemic growth in AML. *Blood*. 2023;142(1):90-105.

31. Tarighat SS, Santhanam R, Frankhouser D, et al. The dual epigenetic role of PRMT5 in acute myeloid leukemia: gene activation and repression via histone arginine methylation. *Leukemia*. 2016;30(4):789-799.

32. Tsherniak A, Vazquez F, Montgomery PG, et al. Defining a cancer dependency map. *Cell*. 2017;170(3), 564.e16-576.e16.

33. Li W, Xu H, Xiao T, et al. MAGeCK enables robust identification of essential genes from genome-scale CRISPR/Cas9 knockout screens. *Genome Biol*. 2014;15(12):554.

34. Zhao M, Kim P, Mitra R, Zhao J, Zhao Z. TSGene 2.0: an updated literature-based knowledgebase for tumor suppressor genes. *Nucleic Acids Res*. 2016;44(D1): D1023-D1031.

35. Challen GA, Pietras EM, Wallscheid NC, Signer RAJ. Simplified murine multipotent progenitor isolation scheme: establishing a consensus approach for multipotent progenitor identification. *Exp Hematol*. 2021; 104:55-63.

36. Cao J, Spielmann M, Qiu X, et al. The single-cell transcriptional landscape of mammalian organogenesis. *Nature*. 2019;566(7745): 496-502.

37. Subramanian A, Tamayo P, Mootha VK, et al. Gene set enrichment analysis: a knowledge-based approach for interpreting genome-wide expression profiles. *Proc Natl Acad Sci U S A*. 2005;102(43):15545-15550.

38. Santana-Codina N, Gableske S, Quiles del Rey M, et al. NCOA4 maintains murine erythropoiesis via cell autonomous and non-autonomous mechanisms. *Haematologica*. 2019;104(7):1342-1354.

39. Georgiades P, Ogilvy S, Duval H, et al. vavCre Transgenic mice: a tool for mutagenesis in hematopoietic and endothelial lineages. *Genesis*. 2002;34(4): 251-256.

40. Qiu X, Mao Q, Tang Y, et al. Reversed graph embedding resolves complex single-cell trajectories. *Nat Methods*. 2017;14(10): 979-982.

41. Rodriguez-Fraticelli AE, Weinreb C, Wang S-W, et al. Single-cell lineage tracing unveils a role for TCF15 in haematopoiesis. *Nature*. 2020;583(7817):585-589.

42. Sommerkamp P, Romero-Mulero MC, Narr A, et al. Mouse multipotent progenitor 5 cells are located at the interphase between hematopoietic stem and progenitor cells. *Blood*. 2021;137(23):3218-3224.

43. Lehnertz B, Chagraoui J, MacRae T, et al. HLF expression defines the human hematopoietic stem cell state. *Blood*. 2021;138(25): 2642-2654.

44. Akashi K, Traver D, Miyamoto T, Weissman IL. A clonogenic common myeloid progenitor that gives rise to all myeloid lineages. *Nature*. 2000;404(6774):193-197.

45. Dixon SJ, Lemberg KM, Lamprecht Michael R, et al. Ferroptosis: an iron-dependent form of nonapoptotic cell death. *Cell*. 2012;149(5): 1060-1072.

46. Mancias JD, Wang X, Gygi SP, Harper JW, Kimmelman AC. Quantitative proteomics identifies NCOA4 as the cargo receptor mediating ferritinophagy. *Nature*. 2014; 509(7498):105-109.

47. Dowdle WE, Nyfeler B, Nagel J, et al. Selective VPS34 inhibitor blocks autophagy and uncovers a role for NCOA4 in ferritin degradation and iron homeostasis in vivo. *Nat Cell Biol*. 2014;16(11):1069-1079.

48. Wang GG, Calvo KR, Pasillas MP, Sykes DB, Häcker H, Kamps MP. Quantitative production of macrophages or neutrophils ex vivo using conditional Hoxb8. *Nat Methods*. 2006;3(4):287-293.

49. Santana-Codina N, Del Rey MQ, Kapner KS, et al. NCOA4-mediated ferritinophagy is a pancreatic cancer dependency via maintenance of iron bioavailability for iron-sulfur cluster proteins. *Cancer Discov*. 2022; 12(9):2180-2197.

50. Perez-Cunningham J, Boyer SW, Landon M, Forsberg EC. Hematopoietic stem cell-specific GFP-expressing transgenic mice generated by genetic excision of a pan-hematopoietic reporter gene. *Exp Hematol*. 2016;44(8):755.e1-764.e1.

51. Gan T, Jude CD, Zaffuto K, Ernst P. Developmentally induced Mll1 loss reveals defects in postnatal haematopoiesis. *Leukemia*. 2010;24(10):1732-1741.

52. Mai TT, Hamaï A, Hienzsch A, et al. Salinomycin kills cancer stem cells by sequestering iron in lysosomes. *Nat Chem*. 2017;9(10):1025-1033.

53. Garciaz S, Guirguis AA, Müller S, et al. Pharmacologic reduction of mitochondrial iron triggers a noncanonical BAX/BAK-dependent cell death. *Cancer Discov*. 2022; 12(3):774-791.

54. Mootha VK, Lindgren CM, Eriksson K-F, et al. PGC-1α-responsive genes involved in oxidative phosphorylation are coordinately downregulated in human diabetes. *Nat Genet*. 2003;34(3):267-273.

55. Meng F, Fleming BA, Jia X, Rousek AA, Mulvey MA, Ward DM. Lysosomal iron recycling in mouse macrophages is dependent upon both LcytB and Steap3 reductases. *Blood Adv*. 2022;6(6):1692-1707.

56. Nielsen J, Gejl KD, Hey-Mogensen M, et al. Plasticity in mitochondrial cristae density allows metabolic capacity modulation in human skeletal muscle. *J Physiol*. 2017; 595(9):2839-2847.

57. Triolo M, Wade S, Baker N, Khacho M. Evaluating mitochondrial length, volume, and cristae ultrastructure in rare mouse adult stem cell populations. *STAR Protoc*. 2023;4(1): 102107.

58. Hackenbrock CR. Ultrastructural bases for metabolically linked mechanical activity in mitochondria. I. Reversible ultrastructural changes with change in metabolic steady state in isolated liver mitochondria. *J Cell Biol*. 1966;30(2):269-297.

59. Quintana-Cabrera R, Mehrotra A, Rigoni G, Soriano ME. Who and how in the regulation of mitochondrial cristae shape and function. *Biochem Biophys Res Commun*. 2018;500(1): 94-101.

60. Cogliati S, Enriquez JA, Scorrano L. Mitochondrial cristae: where beauty meets functionality. *Trends Biochem Sci*. 2016;41(3): 261-273.

61. Chaudhry A, Shi R, Luciani DS. A pipeline for multidimensional confocal analysis of mitochondrial morphology, function, and dynamics in pancreatic β-cells. *Am J Physiol Endocrinol Metab*. 2020;318(2):E87-E101.

62. Hemel IMGM, Engelen BPH, Luber N, Gerards M. A hitchhiker's guide to mitochondrial quantification. *Mitochondrion*. 2021;59:216-224.

63. Ball G, Demmerle J, Kaufmann R, Davis I, Dobbie IM, Schermelleh L. SIMcheck: a toolbox for successful super-resolution structured illumination microscopy. *Sci Rep*. 2015;5(1):15915.

64. Quiros PM, Goyal A, Jha P, Auwerx J. Analysis of mtDNA/nDNA ratio in mice. *Curr Protoc Mouse Biol*. 2017;7(1):47-54.

65. Nakauchi Y, Azizi A, Thomas D, et al. The cell type–specific 5hmC landscape and dynamics of healthy human hematopoiesis and TET2-mutant preleukemia. *Blood Cancer Discov*. 2022;3(4):346-367.

66. Challen GA, Sun D, Jeong M, et al. Dnmt3a is essential for hematopoietic stem cell differentiation. *Nat Genet*. 2011;44(1):23-31.

67. Zhang D, Gao X, Li H, et al. The microbiota regulates hematopoietic stem cell fate decisions by controlling iron availability in bone marrow. *Cell Stem Cell*. 2022;29(2), 232.e7-247.e7.

68. Waarts MR, Mowla S, Boileau M, et al. CRISPR dependency screens in primary hematopoietic stem cells identify KDM3B as a genotype specific vulnerability in IDH2- and TET2-mutant cells. *Cancer Discov*. 2024; 14(10):1860-1878.

69. Lara-Astiaso D, Goñi-Salaverri A, Mendieta-Esteban J, et al. In vivo screening characterizes chromatin factor functions during normal and malignant hematopoiesis. *Nat Genet*. 2023;55(9):1542-1554.

70. Milling LE, Markson SC, Tjokrosurjo Q, et al. Framework for in vivo T cell screens. *J Exp Med*. 2024;221(4):e20230699.

71. Kao YR, Chen J, Kumari R, et al. An iron rheostat controls hematopoietic stem cell fate. *Cell Stem Cell*. 2024;31(3):378.e12-397.e12.

72. Larrue C, Mouche S, Angelino P, et al. Targeting ferritinophagy impairs quiescent cancer stem cells in acute myeloid leukemia

in vitro and in vivo models. *Sci Transl Med*. 2024;16(757):eadk1731.

73. An W, Feola M, Levy M, et al. Iron chelation improves ineffective erythropoiesis and iron overload in myelodysplastic syndrome mice. *Elife*. 2023;12:e83103.

74. Angelucci E, Li J, Greenberg P, et al. Iron chelation in transfusion-dependent patients with low- to intermediate-1–risk myelodysplastic syndromes: a randomized trial. *Ann Intern Med*. 2020;172(8):513-522.

75. Hoelzgen F, Nguyen TTP, Klukin E, et al. Structural basis for the intracellular regulation of ferritin degradation. *Nat Commun*. 2024; 15(1):3802.

76. Yao CH, Wang R, Wang Y, Kung CP, Weber JD, Patti GJ. Mitochondrial fusion supports increased oxidative phosphorylation during cell proliferation. *Elife*. 2019;8:e41351.

77. Jakobsen NA, Turkalj S, Zeng AGX, et al. Selective advantage of mutant stem cells in human clonal hematopoiesis is associated with attenuated response to inflammation and aging. *Cell Stem Cell*. 2024;31(8):1127.e17-1144.e17.